Influence of the microvasculature on oxygen transport in human brain tissue

Shen-Wei SU* and Stephen J. PAYNE

*Corresponding author: Tel.: +44 (0)1865 617660; Fax: +44 (0)1865 617702;
Email: shen-wei.su@eng.ox.ac.uk
Institute of Biomedical Engineering, Department of Engineering Science,
Oxford University, UK

Abstract: Two numerical methods are presented for simulating a micro-stroke: a discretised model and a continuum model, both developed for simulating coupled flow and oxygen transport to the microvasculature. The discrete model treats the microvasculature and the tissue perfusion as two coupled sub-systems governed by Poiseulle flow and mass transport equation respectively. The continuum model regards the blood passage as a porous media flow and deals with mass transport in terms of a two phase flow system. In our simulations, it has been shown that the microvascular structure has a strong influence on the localized oxygen transport behaviour, contributing to more complex patterns in the tissue oxygen concentration than those found by assuming continuum behaviour.

Keywords: Micro Flow, Microcirculation, Dementia, Oxygen transport

1. Introduction

Dementia, a common brain disease, is believed to be attributed to flow-metabolism imbalances in the local microvasculature-tissue network. When a supplying artery becomes blocked, tissue rapidly suffers from a lack of oxygen, a condition termed hypoxia. Smaller infarcts, caused by local damage at the microvessel level, may evolve into large infarcts and cause functional brain damage.

An improved understanding of how the brain responds to micro-infarcts and thus how vascular dementia develops and evolves would be highly beneficial to the improvement of its diagnosis and testament. The study of how the cerebral microcirculation behaves can provide a detailed picture of the flow and mass transport patterns, which can be used to assess localised cell viability. However, our understanding of how such 'micro-strokes' occur is still far from complete, partly due to the limited availability of experimental data concerning the microvasculature properties.

At such length scales, it is unclear whether oxygen transport can be considered as being governed by a continuum flow field or whether the local network properties are important, which is the subject that we address here.

Some researchers believe that the microvasculature plays an important role in oxygen transport in the coupled vessel-tissue system and have tried to investigate the microcirculation based on its morphology and to couple it into tissue oxygen transport. In this category, the classical work in modelling the microcirculatory network was performed by Krogh [1], who suggested that the haemodynamic unit of the microvascular bed is like a bundle of tissue cylinders with the same spatial arrangement. Each cylinder has a capillary located in the centre that supplies oxygen to the nearby concentric tissue area by diffusion as the blood is transported from the arteriole end to the venule end. This model is most likely to apply to tissue where the capillaries pass in nearly the same alignment,

but may not be suitable for tissues perfused by curved vessels with irregular arrangement, as found in the cerebral microvasculature.

Secomb and Hsu [2] considered the tissue as a whole in their analysis of oxygen transport in the skeletal muscle with nearly parallel spaced capillaries and transverse arterioles passing by. The governing equations for oxygen transport were solved using the Green function method and a full three dimensional simulation for tissue oxygen transport was performed. The effects of setting boundary conditions as well as the line source expression on the system oxygen transport were also discussed in later work focusing on oxygen delivery in tissue [3].

A more realistic morphometric model with parallel evenly spaced capillaries having interconnections at random locations was proposed by Beard and Bassingthwaighte [4] for analysis of cardiac tissue. An extension to this model was later proposed by Beard et al. [5] to interpret the experimental data of myocardial oxygen transport in pig heart tissue.

Compared with other tissues, oxygen transport in cerebral tissue has been little investigated through theoretical models. This is partially due to the complexity of the network morphometry. In the cerebral cortex, the microvascular architecture in tissue varies from region to region, which affects the spatial distribution of blood supply. In addition, the regionally varying pattern of neuronal activities affects the consumption rate of oxygen. All these factors are coupled together to contribute to the heterogeneity of oxygen levels in brain tissues, adding extra complexity to any investigations, whether theoretical or experimental.

On the basis of scanning electron micrographs of corrosion casts in rat brain, Secomb et al. [6] reproduced a network with 50 segments. The Green function method was used to predict the oxygen level in the tissues surrounding the network, and the tissue perfusion consumption correlation was also examined. They found that tissue hypoxia coming from perfusion shortage could be alleviated if the oxygen consumption rate in tissue was only moderately decreased.

Considering the flow paths passing through brain tissue to be like voids or small channels, due to their low flow rate condition, we can then describe blood flow motion in the vessel-tissue coupled system by Darcy's Law, which relates linearly the pressure drop across the media to flow velocity [7]. More complicated theoretical models have also been proposed to describe the flow motion in porous media. The patterns of mass diffusion within biological tissue are very different between permeable and impermeable regions due to the influence of blood flow. A comprehensive review of diffusion and other relevant mechanisms in brain tissue was introduced by Nicholson [8], but only the factors affecting the effective diffusivity have been sufficiently addressed. To model the interactions between the haemodynamics and oxygen diffusion in brain tissue, the two phase treatment inspired by Lee and Vafai [9] is thus adopted here for our continuum model, on the basis of classical mass transport equations.

In summary, there are thus two different approaches to the coupled flow-tissue transport problem for brain tissue. The influence of the network sub-model on the mass transport in brain tissue so far remains unclear and the aim of this paper is to uncover the interaction of the blood/tissue coupled system by comparing these two methods modelling the blood delivery accordingly.

2. Method

2.1 Discrete model

2.1.1 Network creation

The first part of our discrete model is the accurate creation of networks to mimic the cerebral microvasculature. The network topology and geometry both highly affect the blood flow circulating in the vessels and hence the oxygen transport to tissue. Since there are very limited topological data available in the

literature relating to the cerebral microvasculature, the experimental study by Cassot et al. [10] is a crucial source of data.

The first step of the network creation is to randomly cluster many nodes in a volume, attempting to reflect the heterogeneity of the branching point distribution in real cerebral networks. Then the connections between nodes are added or removed through different network generating methods by consideration of a range of different factors, such as the node to node distance, the connectivity, or the vessel space density. Several methods including the Shortest Arcs, Gamma Distribution, Spanning Tree and the Modified Spanning Tree Method have been proposed to generate accurate networks whose length distribution and statistical characteristics are close to the experimental results. The network generated by the Modified Spanning Tree Method is found to be the best match to experimental data, as shown in Fig.1 and is adopted here to analyse the influence of network morphology in oxygen transport in the vessel-tissue system as accurately as possible. Full details about the different algorithms and the comparisons between these different network creation methods can be found in a parallel paper [11].

2.1.2 Blood flow in network

The next step is to calculate the blood flow in the network and hence the oxygen transport to and within the surrounding tissue. Due to the low velocity of the blood flow in the microcirculation, the dynamics of the flow are dominated by viscous effects. Thus, for the steady state behaviour, Poiseuille's equation is applied to model the blood flow passing through each vessel, neglecting any possible vessel deformation.

Each vessel in the network is regarded as a solid long uniform tube with constant cross section. Poiseuille's equation implies that the flow is balanced between the pressure drop along the tube and the viscous force:

$$\frac{\Delta P}{Q} = \frac{8\mu L}{\pi r^4} \qquad (1)$$

where Q is volume flow rate (m^3/s), ΔP is the pressure drop across the vessel segment, r is the vessel radius, μ is the dynamic viscosity of the fluid and L is the vessel length. This relationship can be easily extended to model a blood flow network. Eq.1 describes how the pressure drop varies between two nodes, thus for a system with n nodes we can build up a linear system with n unknowns and n equations [12]:

$$Q_i = \sum_j (P_i - P_j)/R_{ij} \quad \text{for} \quad j = 1{:}n \qquad (2)$$

2.1.3 Oxygen transport in network

For a given vessel, considering the steady state only, the modified cross section averaged mass transport equation based on [13] becomes:

$$Q\frac{dC_v}{dx} = -D_w 2\pi r(C_v - C_t) \qquad (3)$$

where Q is the volume flow rate of the vessel, C_v and C_t are the oxygen concentration in the vessel and tissue respectively (in mM) and D_w is the oxygen permeability. Since the vessel is generally short compared to the dimension of the tissue, we assume C_t to vary linearly along the vessel:

$$C_t = \left(C_{ti} - (C_{ti} - C_{to})\frac{x}{L}\right). \qquad (4)$$

We can then obtain the following solution:

$$C = (C_{in} - C_{ti} + \frac{\Delta C}{\lambda L})e^{-\lambda x} + \frac{\Delta C}{L}x + C_{ti} - \frac{\Delta C}{\lambda L} \qquad (5)$$

where $\Delta C = C_{ti} - C_{to}$, and $\lambda = 2\pi r D_w / Q$. Note that the decay constant λ characterizes the oxygen concentration profile along the vessel.

The convection mixing process at a node can be regarded as a weighted combination of the values of all incoming vessels, where j is the index of the starting node in parent vessels converging at node i:

$$C_i = \sum_j C_j Q_{ij} / \sum_j Q_{ij} . \qquad (6)$$

2.1.4 Oxygen transport in tissue

Oxygen transport in brain tissue can be assumed to be governed by the following

equation:

$$\frac{\partial C_t}{\partial t} = D_t \nabla^2 C_t + G_V - M \quad (7)$$

where C_t is the spatially and temporally varying concentration in tissue (mM), D_t is the oxygen diffusivity in tissue (m^2/s), G_V is the net oxygen generation term (mM/s) and M is the tissue consumption associated with brain function (mM/s).

Oxygen diffuses to the tissue from the vessel through the vessel walls, and mass transport in the tissue is thus directly linked with the mass transport in the nearby vessels. Since the oxygen distribution along each vessel can be calculated first, the oxygen extracted from vessels in a given voxel is easily obtained by multiplying the flow rate and the concentration drop between the terminal points at the surfaces. G_V is then determined by calculating the total oxygen flux from vessels in every voxel. On the other hand, the sink term M reflects the tissue oxygen consumption and is set to be constant according to the assumption made by Beard [13].

2.2 Continuum model

2.2.1 Flow in network/tissue

If the network is not modelled directly, the brain tissue can be treated as a porous medium with many tortuous flow channels or voids. Due to the low flow velocity in the real network, the steady state blood flow motion in tissue can be taken to be governed by Darcy's flow equations [7]:

$$\mathbf{q} = -\frac{\mathbf{K}}{\mu}\nabla P = \frac{\mathbf{V}}{\varphi} \quad (8)$$

where $\mathbf{q}$ and ∇P are the Darcy velocity and the pressure gradient respectively. $\mathbf{V}$ is the flow field and φ is the porosity. The Darcy velocity is divided by porosity to incorporate the fact that only a fraction of the total formation volume is available for flow. Although, the permeability $\mathbf{K}$ is a second order symmetric tensor, representing the directional transport variations, here we assume that it is constant under the assumption of an isotropic medium.

2.2.2 Oxygen transport in blood/tissue

Since the flow is passing through the tissue, the oxygen transport in blood and tissue must be coupled properly. Here we consider the vessel tissue system as a two phase flow system, Lee and Vafai [9], including the blood flow perfusion through all areas occupied at a volume fraction of ϕ_b and the tissue represented by a static fluid with volume fraction ϕ_t ($\phi_b + \phi_t = 1$) as shown in the following equations:

$$\phi_b\left(\frac{\partial C_b}{\partial t} + (\mathbf{V}\cdot\nabla)C_b\right) = G_V \quad (9)$$

$$\phi_t \frac{\partial C_t}{\partial t} = \phi_t D_t \nabla^2 C_t - G_V - \phi_t M \quad (10)$$

$$G_V = -\phi_b D_w (2/r_e) \times (C_b - C_t) \quad (11)$$

The oxygen concentrations in blood and tissue are represented by the C_b and C_t respectively. All other terms are the same with those introduced in discrete model except for r_e, representing the effective vessel radius. The blood and tissue oxygen transport equations are thus coupled together.

Apart from calculation of flow patterns in discrete model, flow and mass transport equations for both models are all discretised by the finite volume method, which has been widely used in solving heat and mass transfer equations [14].

3. Result and discussion

In both flow simulations considered here, two flow sources and two flow sinks are put in a $(0.5mm)^3$ cube at the following locations ((0.1,0.1,0.1); (0.4,0.1,0.4); (0.1,0.1,0.1); (0.4,0.1,0.4)) to mimic the arteriolar inlets and venous outlets in the microvascular bed with flow input and output. For the discrete model, the blood pressure at inlet and outlet in the vascular network is set to be 3000Pa and 1000Pa respectively, resulting in a total inlet flow rate of 2.49×10^{-13} m^3/s, which is also set to be the flow source strength for solving Darcy's equation in the continuum model.

For both models, the boundary conditions for oxygen concentration in the tissue are the same: in the y and z directions there is no flux whilst in the x direction concentration is set to be a constant:

$$C(0, y, z) = C(l, y, z) = 0.1\text{mM}$$

$$\frac{\partial C(x,0,z)}{\partial y} = \frac{\partial C(x,l,z)}{\partial y} = 0$$

$$\frac{\partial C(x,y,0)}{\partial z} = \frac{\partial C(x,y,l)}{\partial z} = 0$$

The oxygen concentration at the sources for solving the blood delivery equations in both cases is taken as 10mM and the initial concentration for the oxygen concentration in both blood and tissue is set at 0.1mM. The boundary conditions for the porous flow are set to be zero flux at all walls. To simulate a mini-infarct caused by blood flow shortage, a vascular blockage is mimicked by disabling one flow source at 200s. Eight symmetrically arranged points are chosen in this model to monitor the temporal behaviour of tissue oxygenation in response to this reduction.

In Fig.1, an artificial network created according to the Modified Spanning Tree Method [11] shows the considerable heterogeneity in vessel distribution. The network architecture is not well organized with an order that parent and children vessels can be easily defined. Instead, it shows a web-like structure shared with the real microvascular network observed recently [10].

From the oxygenation time course comparison between the two models as shown in Fig.2, the spatially averaged oxygenation can be seen to be higher in the discrete model. Both curves rise up rapidly to reach an equilibrium state, dropping sharply as the flow blockage occurs, finally settling down to a new steady state and interestingly they all have a drop around 0.1 after one flow source is removed.

The tissue concentration contours for discrete and continuum models are shown in Fig.3 and Fig.4 respectively. The concentration distributions for both cases share similar geometric features, and their oxygen levels decay gradually with the distance from the sources to the two sinks. Oxygen is transported further in the discrete model since its contours cover a larger area than do those in the continuum model. In addition, for the discrete model, a higher oxygen level can be found in the region closed to sources. In all, the oxygen level is higher in discrete model, which is in coherent with curves showing the time course comparison between two models.

Unlike the geometric symmetry of contours found in the continuum model, due to the irregular mass transport in vessel network, there is very weak symmetry seen in the oxygen contour in the discrete model. This flow induced asymmetry may result from the unevenness in the network distribution, indicating that the network affects a great deal on the mass transport pattern in tissue.

For both cases, after one flow source is disabled, oxygen in the surrounding area cannot be sustained at a high level, declining dramatically to the baseline value (0.1mM), as shown by the shrinkage of the oxygen contour in Fig. 3 and 4. In Fig. 3, the concentration contour supplied by the one remaining source seems simply to be split from the double contour pattern existing before source removal, but this is not a feature that is shared with the discrete model. The resulting contour, shown in Fig.4, has a larger region at high oxygen levels than the previous one, due to the flow redistribution after one source is removed. This implies that there is some local concentration increase in specific regions that benefit from the flow path rearrangement in the vessel network even if the net oxygen input is reduced.

Fig.5 and Fig.6 show the time course of the averaged tissue oxygenation levels for both discrete and continuum models at eight symmetric arranged points C1-C8 (note that C1-C4 are in the plane spanned by the two source and sinks while C5-C8 are perpendicular to the source sink plane).

As shown in Fig.5, the oxygen levels at these

monitoring points do not always undergo a decrease after the source removal. For example, the oxygen levels at C1 and C3 have an increase rather than a decrease. This could be attributed to the change in the oxygenation induced by flow pattern changes in response to the source removal at 200s. Since oxygen exchange at the vessel wall is proportional to the vessel-tissue concentration difference, the increase in wall exchange can be achieved by flow rearrangement. In particular, when flow reversal occurs, the pressure drop between the vessel and the tissue becomes larger or the flow rate along a vessel increases. All these effects can contribute to a higher wall exchange in local areas even when the total system influx is greatly reduced.

In Fig.6, before the source removal, two pairs of curves coincide with their counterparts due to the symmetric arrangement. After one of the sources is removed, the coinciding curve pairs (C5-C6; C7-C8) no longer exhibit the spatially symmetric field found previously. The point near the removed source has a larger drop than that of its symmetric counterpart. Comparison between the curves for C5 and C7 also indicates that the closer the point is to the removal source, the larger concentration drop it will have after a flow reduction.

4. Conclusion

A discrete model and continuum model are presented here to simulate the flow and oxygen transport in brain tissue. The time history for averaged oxygenation for both models reveals synchronized system states while that for tissue oxygenation at different locations share the similar state transition patterns. The continuum model can capture basic mass transport patterns as does the discrete model. In addition, as the flow blockage occurs, the region near the removed source is unable to maintain sufficient oxygen supply, leading to a significant decrease in oxygen level.

However, the discrete model considers the detailed network information, capturing the spatially-varying flow patterns which lead to inhomogenous oxygen flux to the tissue. Some oxygen transport features, such as unexpected local oxygen level increases induced by flow redistribution can only be shown in this model.

The significance of the flow source can be found in the mass transport to brain tissue. The convective transport is not sufficient to bring oxygen to sites remote from the supply, even at this length scale, leading to a significant oxygen shortage. This implies that the density of the flow sources must be well set to meet the physiological demand.

The influence of changes of flow distribution on the oxygen transport in tissue indicate the strong influence of the local microvascular structure, leading to the more complex patterns in oxygenation found in the discrete model than in the continuum model. Therefore, detailed morphometric analysis for vascular network is a very valuable requirement for future simulations, such as those conducted by Su et al. [11].

At this stage, due to the lack of information concerning the flow rate and locations of the artery-capillary and vein-capillary junctions, we cannot thus interpret the exact nature of this flow yet. In addition, the permeability, porosity and oxygen diffusivity in tissue need to be considered in more detail in the light of physiological measurements to yield a more detailed and accurate understanding of the real system.

Reference

[1] A. Kough, 1921,Studies on the physiology of capillaries. II. The reactions to local stimuli of the blood vessels in the skin and web of the frog. *J. Physiol.* 55:414–422.

[2] T. W. Secomb, and R. Hsu, 1994. Simulation of oxygen transport in skeletal muscle: diffusive exchange between arterioles and capillaries. *Am. J. Physiol*. 267: H1214-1221.

[3] T. W. Secomb, R. Hsu, E.Y.H. Park, and M. W. Dewhirst, 2004, Green's function methods for analysis of oxygen delivery to tissue by microvascular networks. *Ann. Biomed. Eng*, 32: 1519-1529.

[4] D. A. Beard and J. B. Bassingthwaighte, 2001. Modeling advection and diffusion of oxygen in complex vascular networks, *Ann. Biomed. Eng*. 29: 298–310.

[5] D. A. Beard , K. A. Schenkman and E. O. Feigl, 2003. Myocardial oxygenation in isolated hearts predicted by anatomically reasonable microvascular transport model. *Am. J. Physiol.* 285: H1826-H1836, 2003.

[6] T.W. Secomb, R. Hsu, N. B. Beamer, and B.M. Coull, 2000. Theoretical simulation of oxygen transport to brain by networks of microvessels: effects of oxygen supply and demand on tissue hypoxia. *Microcirculation* 7: 237-247

[7] H.R.P.G. Darcy, 1856, Les Fontaines Publiques de la volle de Dijon, Vector Dalmont, Paris.

[8] C. Nicholson, 2001, Diffusion and related transport mechanismin brain tissue, *Rep. Prog. Phys*. 64, 815–884.

[9] D.Y. Lee, K. Vafai,1999, Analytical characterization and conceptual assessment of solid and fluid temperature differentials in porous media, *Int. J. Heat Mass Transfer* 42, 423–435.

[10] F. Cassot, F. Lauwers, C. Fouard, S. Prohaska and V. Lauwers-Cances, 2006. A novel three-dimensional computer-assisted method for a quantitative study of microvascular networks of the human cerebral cortex, *Microcirculation* 13 : 1–18.

[11] S. Su, M. Catherall and S. Payne, 2009, A novel computational algorithm for the generation of network models based on their statistical properties, Manuscript in preparation.

[12] H.H. Lipowsky and B.W. Zweifach, 1974. Network analysis of microcirculation of cat mesentery. *Microvasc Res.* 7:73-83.

[13] D. A. Beard , 2001. Computational framework for generating transport models from databases of microvascular anatomy. *Ann. Biomed. Eng*. 29:837-843.

[14] S. V. Patankar,1980. Numerical Heat Transfer and Fluid Flow, Hemisphere, Washington, DC. USA.

TABLE I
UNITS FOR PROPERTIES

Symbol	Quantity	Unit
μ	Blood dynamic viscosity	3×10^{-3} kg s/m
D_w	Wall oxygen permeability	5.5×10^{-6} m/s
D_t	Tissue oxygen diffusivity	1×10^{-9} m^2/s
K	Permeability	1×10^{-9} m^2
M	Oxygen consumption	0.005 mM/s
φ	Porosity	0.03
Φ_b	Blood volume fraction	0.03

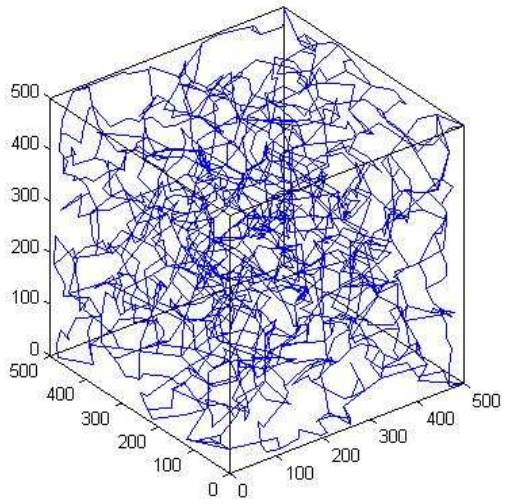

Fig. 1 Artificial network created by Modified Spanning Tree Method

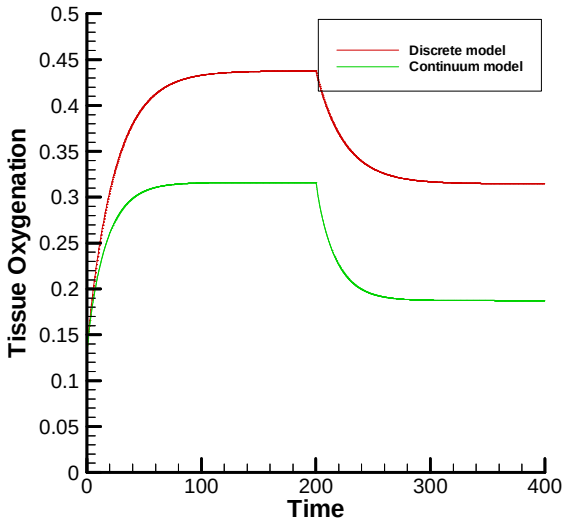

Fig. 2 Time course of spatial averaged tissue oxygenation (in mM) for the discrete and continuum model

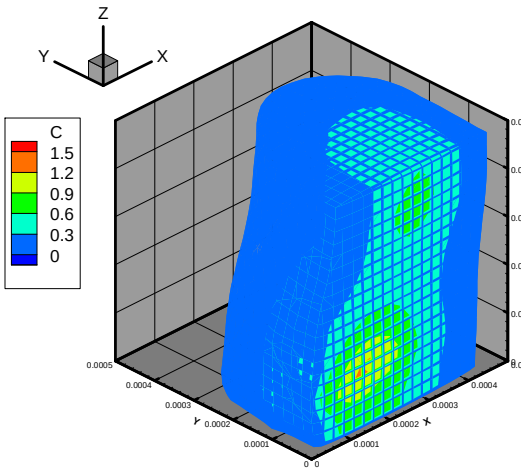

Fig. 3 Oxygen contours (in mM) in the discrete model: above is the contour at 200s; below the contour at 400s

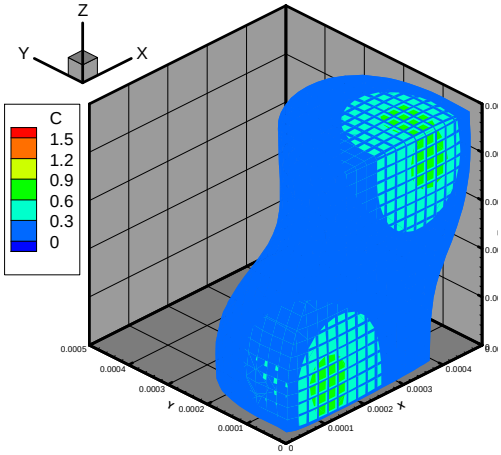

Fig. 4 Oxygen contours (in mM) in the continuum model: above is the contour at 200s; below the contour at 400s

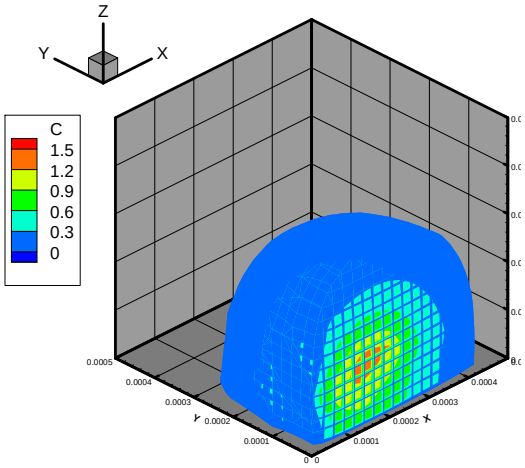

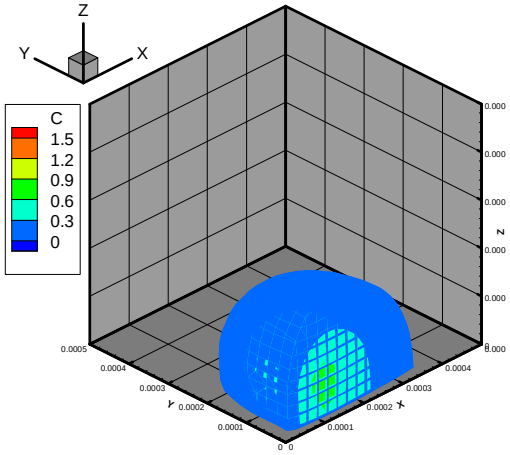

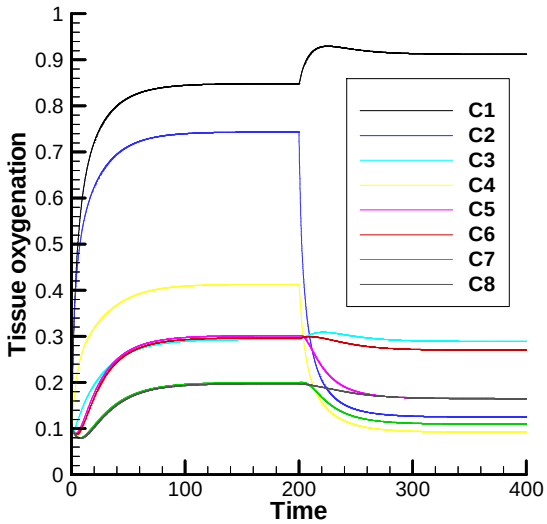

Fig. 5 Time course of tissue oxygenation (in mM) for discrete model at monitored points

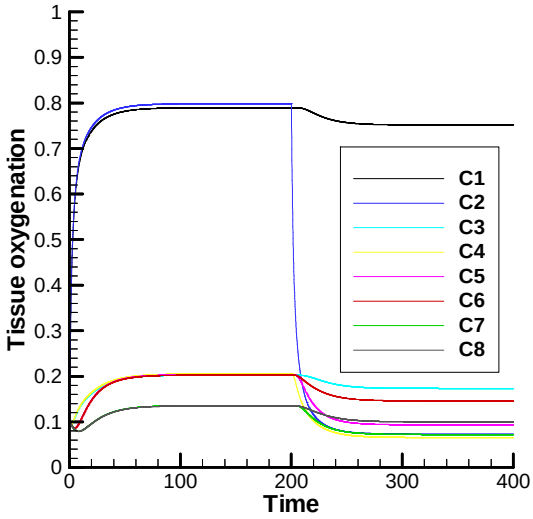

Fig. 6 Time course of tissue oxygenation (in mM) for continuum model at monitored points